Macromolecules

pubs.acs.org/Macromolecules Article

Side Chain Dipole Orientation and Its Effect on Microphase Separation: Experiment and Simulation via Structural Isomer Variation

Hongbo Feng, Ludwig Schneider, Whitney Loo, Gordon S. W. Craig, Christopher Eom, Zhongyang Wang, Ricardo Ruiz, Juan J. de Pablo,* Stuart J. Rowan,* and Paul F. Nealey*

Cite This: *Macromolecules* 2023, 56, 4591−4601 Read Online

ACCESS | Metrics & More | Article Recommendations | Supporting Information

ABSTRACT: We use experiments and molecular dynamics simulations in an investigation of structural isomer−property relationships in block copolymers (BCPs) that allow us to isolate the effects of dipole orientation on microphase separation and χ. We combine anionic polymerization of a single parent BCP with post-polymerization thiol-epoxy "click" chemistry with a series of structural isomers of fluorinated thiophenols to synthesize structural isomeric BCPs (SI-BCPs). The resulting SI-BCPs possess identical molecular weight and dispersity, such that only the isomerism can affect microphase separation. Domain periodicity of the SI-BCPs is measured with small angle X-ray scattering, from which χ is estimated. The value of χ for each SI-BCP shows a significant dependence on the position of fluorine atoms on the phenyl ring of the thiophenol. Simulation results show a strong correlation between the dipole moment orientation of the appended thiol and χ, which is also observed in simulations of a BCP of the structural isomers poly(2-vinylpyridine) and poly(4-vinylpyridine). This work illustrates a little-known facet of the structure−property relationship of BCP materials and provides another tool for the molecular engineering of BCPs.

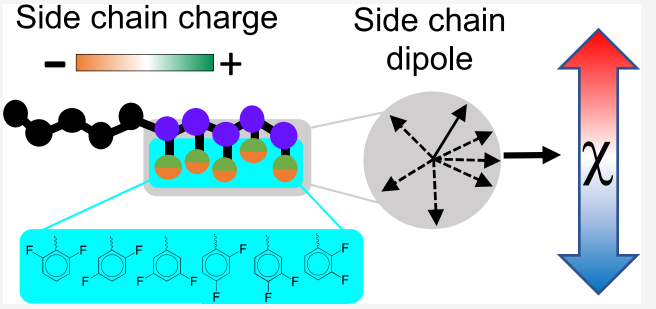

INTRODUCTION

Isomerism refers to molecules having the same number and types of atoms but arranged in a different manner. In polymers isomerism can be classified into three general categories: structural isomerism, stereoisomerism (tacticity), and sequence isomerism.[1] The chemical complexity and vast number of repeat units in a polymer chain has led to the interpretation of isomerism as a collective interaction between multiple isomeric units. Synthetic polyisoprene, for example, possesses four isomeric microstructures, *i.e.*, 1,2-, 3,4-, *cis*-1,4-, and *trans*-1,4-, where the ratio of these microstructures can be controlled through polymerization conditions.[2,3] Structural isomers of polyisoprene consisting of various ratios of these microstructures exhibit drastically disparate properties. *cis*-1,4-Polyisoprene is the major component of natural rubber, with a typical tensile strength of 17−25 MPa and a typical glass transition temperature (T_g) of −70 °C,[3,4] while 3,4-polyisoprene is much stiffer and has a higher T_g, −16 °C.[5] Block copolymers (BCPs) consisting of chemically distinct segments have attracted considerable attention experimentally and theoretically[6,7] because of their ability to self-assemble into a wide range of nanostructures and their use as scaffolds for a variety of applications including directed self-assembly for lithography,[8−11] drug delivery,[12] and the fabrication of porous membranes.[13,14] The morphologies and domain spacing of these nanostructures are determined by the Flory-Huggins interaction parameter (χ), the number of statistical segments in the polymer chain (N), and the volume fraction (f), which can be manipulated by joining chemically distinct blocks or monomers.[6] Polyvinyl pyridines are widely studied in the context of structurally isomeric BCPs (SI-BCPs). Polystyrene-*block*-poly(2-vinyl pyridine) (S-*b*-P2VP) has a χ of 0.1 while polystyrene-*block*-poly(4-vinylpyridine) (S-*b*-P4VP) exhibits a much higher χ of 0.4 under similar annealing conditions.[15,16] Even poly(2-vinylpyridine)-*block*-poly(4-vinylpyridine) (P2VP-*b*-P4VP) can undergo microphase separation with a χ of 0.26 at 150 °C.[17] Chain mobility of the two isomers of PVP is also notably different, as indicated by the distinct T_gs of P2VP (∼100 °C) and P4VP (∼140 °C).[18] These drastically different properties are most likely attributed to the position of the nitrogen atom on the aromatic ring, where the nitrogen atom of 2VP is closer to the hydrocarbon backbone than that

Received: April 5, 2023
Revised: May 17, 2023
Published: June 15, 2023

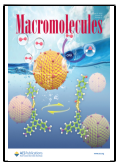

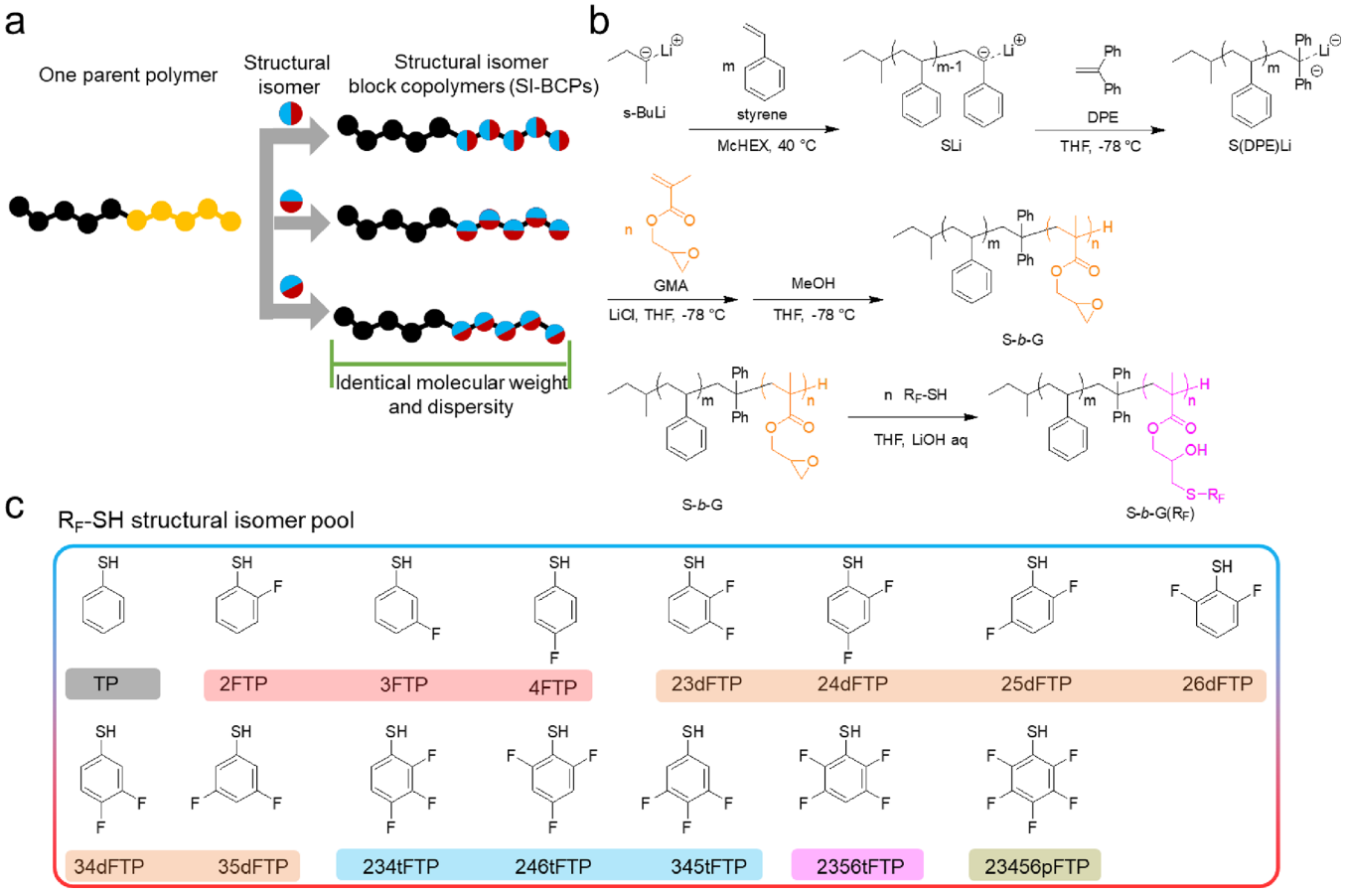

Figure 1. (a) Design of well-defined block copolymers (BCPs) modified with different structural isomers, such that the resulting structural isomer BCPs have identical molecular weight and dispersity. (b) Chemistry platform and synthetic scheme for the polymerization of polystyrene-*block*-poly(glycidyl methacrylate) (S-*b*-G) BCP and its modification with fluorinated thiophenol (R_F-SH) structural isomers to form thiol-modified polystyrene-*block*-poly(glycidyl methacrylate) (S-*b*-G(R_F)). (c) R_F-SH pool consists of mono-, di-, tri-, tetra-, and pentafluorine-modified thiophenols. The abbreviation of each thiol is labeled. Nonfluorinated thiophenol (TP) is used as a control.

of 4VP. Poly(3-vinylpyridine) is rarely reported, possibly due to synthetic challenges. Nonetheless, it is apparent that incorporating structural isomerism into BCPs can lead to delicate thermodynamic changes and differences in self-assembly behavior.

A deeper understanding of the effects of structural isomerism on BCP thermodynamics is important. For synthetic polymers, however, variations in molecular weight (M_n) and dispersity ($Đ$) can obscure the effects of structural isomerism. It is thus helpful to develop a high-precision structural isomer block copolymer (SI-BCP) platform with identical M_n and $Đ$ amongst all samples to elucidate the impact of structural isomerism. A strategy that relies on well-defined polymer precursors modified with structural isomeric small molecules offers an ideal platform for a systematic study of structural isomers. Living anionic polymerization techniques are the gold standard to produce a single batch of well-defined polymer precursors. "Click" chemistry provides an ideal modification approach because of its 100% atom efficiency and high regio-selectivity.[19,20] If different parts of the same batch of polymer are modified with different structural isomers, it is expected that the resulting structural isomeric polymers will exhibit identical M_n and nearly equal, if not identical, $Đ$.

Here, we propose a precision chemistry platform that combines well-defined polymers synthesized via living anionic polymerization and a modification via thiol-epoxy "click" chemistry.[21] The polymer used in this work is polystyrene-*block*-polyglycidyl methacrylate (S-*b*-G). Fluorine-containing thiophenol (R_F-SH) structural isomers are used to modify S-*b*-G. The "click" reaction has high regioselectivity as the thiolate anion only attacks the less hindered carbon of the epoxy ring under our selected reaction conditions.[22] The resulting SI-BCPs (S-*b*-G(R_F)) have identical M_n and $Đ$, with the only difference being the number of fluorine (F) atoms and their position on the phenyl ring. The self-assembly behavior, morphology, and domain periodicity in the melt are investigated using small-angle X-ray scattering (SAXS). Chain conformation and statistical segment length (a) are evaluated from the radius of gyration (R_g), measured with SAXS, and the hydrodynamic radius (R_h), measured with viscometry. The impact of structural isomerism on χ of S-*b*-G(R_F) is measured and, by relying on detailed simulations of the underlying materials, a correlation between χ and dipole moments induced by the R_F isomer is established.

RESULTS AND DISCUSSION

Figure 1 outlines the design and detailed chemistry platform of the SI-BCPs. In this design, a well-defined parent polymer, S-*b*-G, was first synthesized via living anionic polymerization.[23] The details of the synthetic procedure and characterization can be found in the experimental section and Supporting Information, Figure S1. A lamellar morphology was selected

https://doi.org/10.1021/acs.macromol.3c00630
Macromolecules 2023, 56, 4591−4601

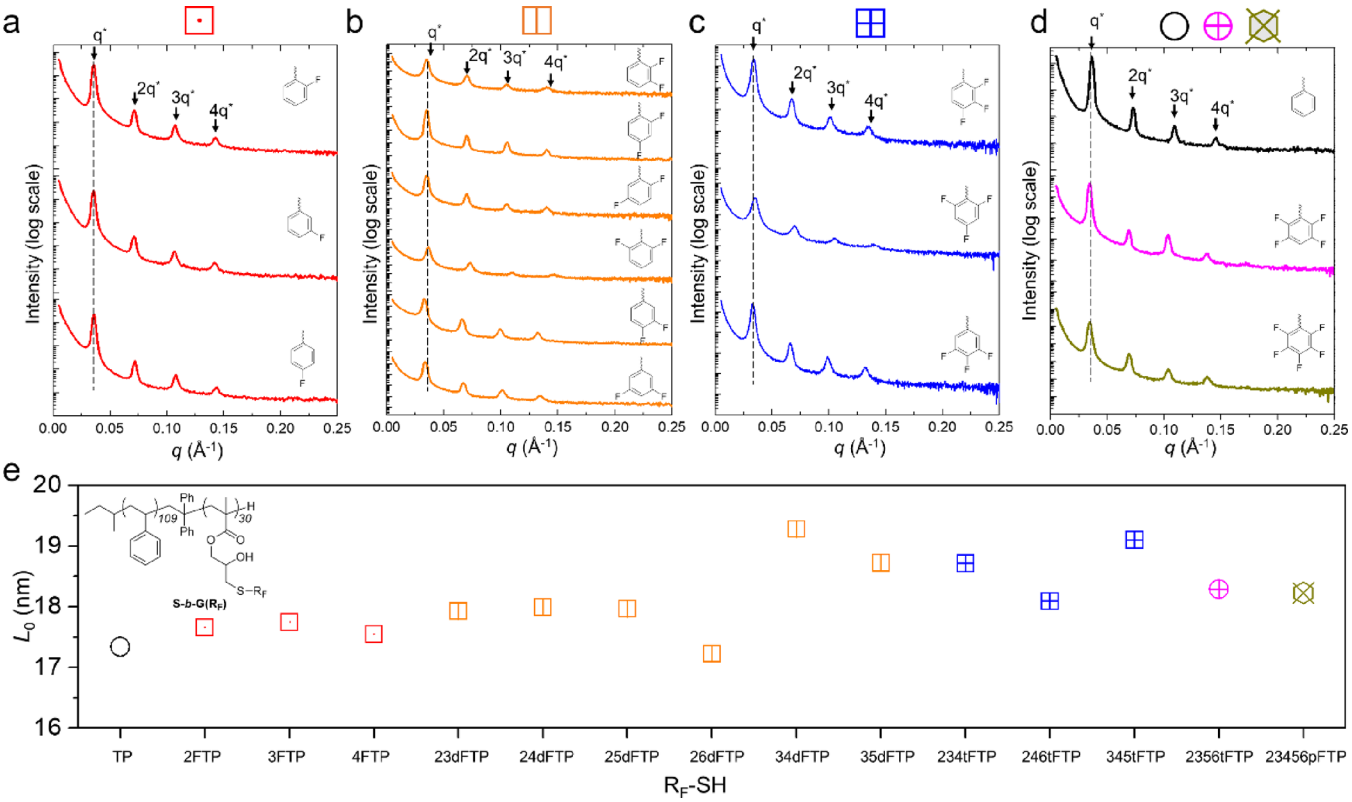

Figure 2. (a–d) Stacked SAXS profiles of S-*b*-G(R_F) after annealing in identical conditions. All profiles show a lamellar morphology with characteristic scattering peaks labeled. The chemical structures of the corresponding R_F are included for each profile. A vertical black dashed line in each figure is used to guide the eye, showing the deviation of the location of q^*, the principal Bragg reflection peak. (e) Lamellar periodicity (L_0) of each S-*b*-G(R_F) is indexed by the corresponding R_F-SH.

for this study, and the volume fraction of S (f_S) in the parent polymer, S_{109}-*b*-G_{30} (the subscripts represent the average degree of polymerization in each block), was controlled to be S-rich (f_S = 0.72) to compensate for the increase in volume of the G block caused by the addition of the thiols after the click reaction (f_S = 0.56 after reaction). A series of structural isomers, fluorinated thiophenols (R_F-SH), were then used to modify the S-*b*-G *via* the thiol-epoxy "click" reaction, generating a series of well-defined S-*b*-G(R_F) with identical degrees of polymerization and M_n (e.g., S-*b*-G modified with 2,6-difluorothiophenol (26dFTP) or 3,4-difluorothiophenol (34dFTP) to make S-*b*-G(26dFTP) or S-*b*-G(34dFTP), respectively) and $Đ$, with the only difference being the position of F atoms on the aromatic ring. The results of the characterization of these SI-BCPs, including M_n and $Đ$ of S-*b*-G(R_F), can be found in the Supporting Information, Figures S2–S7 and Table S1. The BigSMILES line notation for these BCPs is shown in Table S4.[24] This library of S-*b*-G(R_F) materials allows for a systematic investigation of the effect of structural isomerism on the self-assembly of BCPs.

To investigate the morphology and domain periodicity of self-assembled S-*b*-G(R_F), these polymers were subjected to identical annealing conditions (150 °C for 20 h under vacuum) followed by bulk transmission SAXS measurements. An annealing temperature of 150 °C was selected because it was above the T_g of the BCPs but below their degradation temperature, as determined by differential scanning calorimetry (DSC). Because no epoxy groups remained after the thiol-epoxy reaction, as determined by nuclear magnetic resonance spectroscopy (^{1}H NMR), there was not a risk of the G block cross-linking at 150 °C. Figure 2a–d shows the SAXS profiles of the mono-, di-, tri-, and pentafluorine-modified S-*b*-G(R_F), respectively, where the scattering peaks correspond to a lamellar morphology, as designed. The lamellar periodicity ($L_0 = 2\pi/q^*$, where q^* is the principal Bragg reflection) changed with respect to the number and position of F atoms in the phenyl ring (Figure 2e). Specifically, the L_0 values of the SI-BCPs that contained two F varied from 17.1 to 19.2 nm, with the change in L_0 depending solely on the position of the F atoms. S-*b*-G(26dFTP) had the lowest L_0 of 17.1 nm, and S-*b*-G(34dFTP) had the largest L_0 of 19.2 nm.

Strong segregation theory (SST) predicts that[25]

$$L_0 = 1.10aN^{2/3}\chi^{1/6} \quad (1)$$

where N is determined using a reference volume of 144 Å^3, as described in the Supporting Information. The BCPs in our study are unlikely to be in the strong segregation regime, where $\chi N \geq 100$. However, previous work has found that eq 1 yields good estimates even for $\chi N < 20$.[26,27] Moreover, we expect that the deviation from SST of these BCPs is systematic, given that the BCPs are identical except for the structural isomerism of the pendant thiols. This relationship allows us to evaluate the impact of isomerism by connecting L_0 with χ. Indeed, the purpose of our estimation of χ values is to evaluate any effects that isomerism may have on χ. Therefore, while methods such as the random phase approximation are better for determining definitive values of χ,[28,29] our approach here is sufficient for an internally consistent study of the effects of isomerism on χ. Here, we assume that the density of G(R_F), if isomers are used, is identical and therefore N is identical. The densities are

https://doi.org/10.1021/acs.macromol.3c00630
Macromolecules 2023, 56, 4591–4601

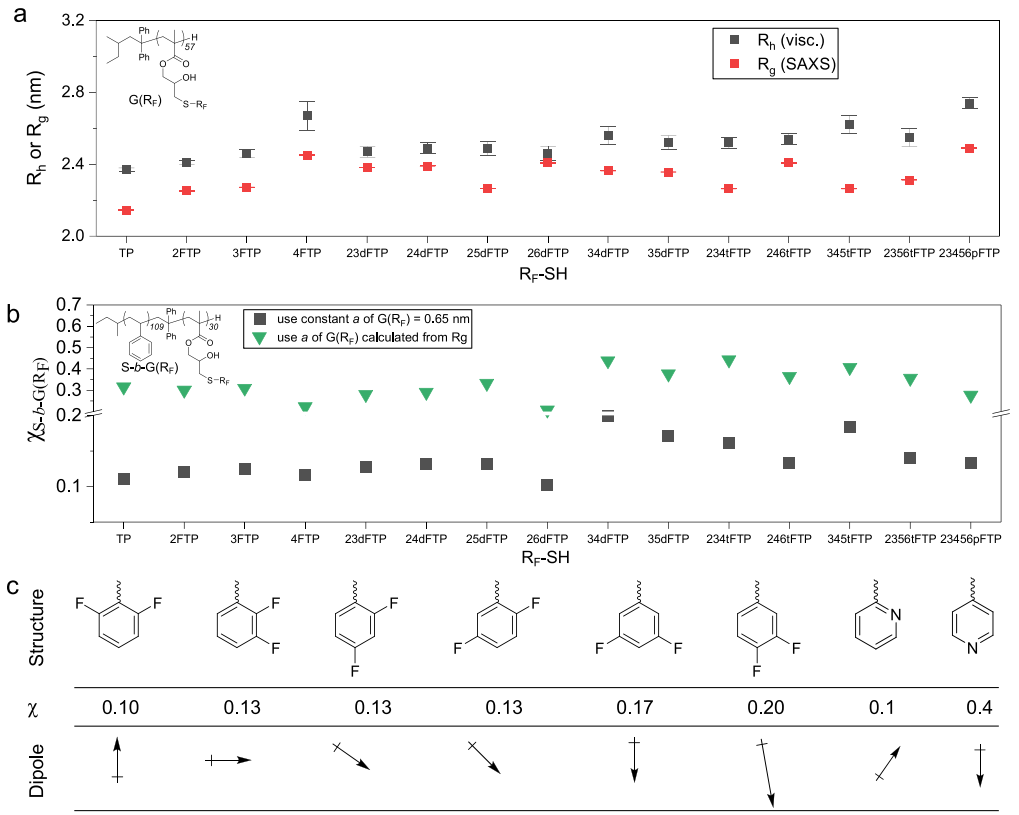

Figure 3. (a) Hydrodynamic radius (R_h) and radius of gyration (R_g) of the different G(R_F) homopolymers measured in THF using a viscometer and SAXS, respectively. Although the chain confirmation of G(R_F) is in a perturbed state, the chain dimensions of the different G(R_F) isomers are close to each other; hence, we assume that the *a* of G(R_F) is constant. (b) Calculated values of $\chi_{S\text{-}b\text{-}G(RF)}$ indexed by the corresponding R_F-SH. The bulk S-*b*-G(R_F) were annealed in identical conditions, 150 °C for 20 h under vacuum. Two calculated values are shown: one with a constant *a* value, and one with an *a* value determined form the corresponding R_g value in (a). (c) Correlation between dipole direction of the pendant fluorinated phenyl ring and χ in a difluorine-modified S-*b*-G. The dipole vectors are only drawn as a guide to the eye. An increasing χ was obtained as the dipole orientation changed from upward (towards the C−C backbone) to downward (away from the C−C backbone). The last two entries are for the structural isomers of a block copolymer of S and vinylpyridene (S-*b*-P2VP and S-*b*-P4VP), which exhibit a similar trend. The χ values are from Kennemur's review article.[35]

estimated using Parachor parameters and are listed in Table S2.[30]

We also assumed that modification of G using different isomers of R_F-SH does not change the value of *a* of G(R_F). To substantiate the second assumption, the chain dimensions including R_g and R_h of G(R_F) in THF were measured using SAXS and a viscometer coupled with a GPC, respectively (Figure 3a). Additional details can be found in the Supporting Information (Figures S9−S12 and Table S3). It should be noted that the actual value of *a* is determined with the polymer in a theta solvent, which can be attained using a mixture of a non-deuterated polymer and its deuterated counterpart.[31,32] In the case of difluorine-modified G, the largest differences in R_g and R_h were 7 and 6%, respectively. Because the R_g/R_h values for the different G(R_F) polymers (Table S3) had less variation than has been reported for standard polymers in non-theta solvents,[33] we concluded that it would be acceptable to use the R_g data to determine the trend of *a* as well as an estimate of *a*. However, because we were uncertain of the exact *a* value, we calculated a pair of χ values for each of the corresponding R_F-SH, using eq 1 with either *a* = 0.65 nm for all G(R_F) or *a* determined from the R_g value and *N* of each G(R_F).[34] As shown in Figure 3b, across the range of the R_F-SH, each pair of χ values varied in approximately the same way. Because the difference in L_0 was larger (∼12%) than R_g or R_h and, more importantly, uncorrelated with R_g, with an absolute value of the Pearson correlation coefficient *R* of only 0.027 (Figure S13 in the SI), we assumed a constant value of *a* = 0.65 nm for all subsequent calculations of χ from measured L_0 values.

Computer simulations can be used to determine the stiffness with considerable computational effort. In the Supporting Information, Figures S17 and S18, we include an analysis of three example systems, where we determine χ with stiffness values determined from computer simulations. In this analysis, we also use an extended SST that takes the asymmetric stiffness of the two blocks into account. As a result, we find the same correlation as that obtained from the simpler analysis, which is used for the remainder of the manuscript, as shown in Figure S18. We conclude that the difference in L_0 is mainly attributed to the differences in χ.

The differences in χ can be directly attributed to the difference in the underlying chemical structures of S-*b*-G(R_F), namely, the position of the F atoms on the phenyl ring, which alters the dipole moment of the phenyl moiety because of the strong electron-withdrawing effect of F. This results in changes to the charge distribution and the dipole moment of the side chain, particularly the phenyl ring, as shown in Figure 3c. To investigate the correlation between the dipole moment of G(R_F), including its orientation and magnitude, and χ, we performed atomistic computer simulations that incorporate the

https://doi.org/10.1021/acs.macromol.3c00630
Macromolecules 2023, 56, 4591−4601

partial charges of the atoms. A typical bulk simulation representative configuration is shown in Figure 4.

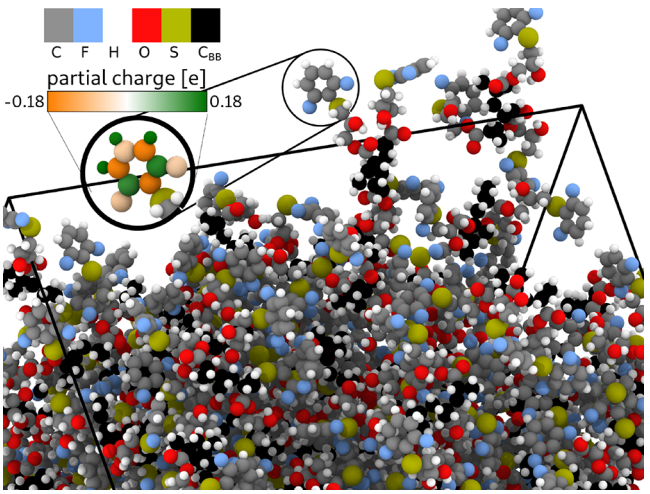

Figure 4. Representative configuration of a simulated 3-mer bulk system G(26dFTP), with low χ. Atoms are drawn without periodic boundary conditions to guide the eye toward individual molecules. The bulk is a dense liquid. In addition to the color coding of the atoms shown in the legend, the carbon atoms of the backbone are shown in black. A single phenyl ring is enlarged and colored to demonstrate that the simulation can access the partial charges on the ring. An animated version of the generation of the configuration is supplied in the online version.

Figure 4 shows that the simulation can access the partial charge along the side chains of polymer chain, and the effects of the partial charge distribution and the relation of the dipole moment of the side chains to the backbone of the polymer chain are of particular interest. To investigate these effects, schematics of a 3-mer from the bulk simulation of each difluorine-modified S-*b*-G(R_F) were generated to visualize the partial charge distribution, with a 3-mer of G(34dFTP) shown as an example in Figure 5. Figure 5b reveals how partial charges are arranged along the 3-mer atoms. As one might expect, the oxygen atoms carry the largest partial charges and have a strong influence on the total dipole moment. However, for all isomers, the effect of the oxygen atoms remains approximately the same because only the F atoms on the phenyl ring change. Their effect on the ring can be seen by comparing the charges of the phenyl ring of G(26dFTP) in Figure 4 to those of G(34dFTP) in Figure 5c (right). While the total partial charge differences are not significant, the orientation between the charge distribution of the phenyl ring with respect to the sulfur atom that connects to the backbone is highly significant, with the phenyl ring of G(26dFTP) having more partial charge close to the sulfur atom than G(34dFTP) does.

To further analyze the effect of the distribution of partial charges on the phenyl ring, the simulated bulk configurations were used to understand the effect of the dipole moment vector $\vec{d}$ of the phenyl ring and the orientation of the monomer side chain $\overrightarrow{br_{cm}}$ relative to the polymer backbone, as shown in Figure 6. The vector $\overrightarrow{br_{cm}}$ points from the center of mass of the side chain to the midpoint between the two carbon atoms of the monomer building the backbone. Of particular interest is the orientation $\vec{d}$ with respect to $\overrightarrow{br_{cm}}$ and to the direction to the polymer backbone. The vector $\overrightarrow{br_{cm}}$ allows us to describe the relationship between the monomer and the dipole moment in a translationally and rotationally invariant manner. The angle α between $\vec{d}$ and $\overrightarrow{br_{cm}}$, shown in Figure 6, provides a magnitude invariant description, while the inner product between both vectors, $s = \overrightarrow{br_{cm}} \cdot \vec{d}$, considers magnitudes and orientations.

The bulk system simulations of 3-mers can be used to systematically investigate the angle, α, the inner product, s, and their relationship for all possible positions of the fluorine atoms on the phenyl ring of the difluorine-modified S-*b*-G(R_F). Such an investigation provides into the 3-dimensional relationship between $\vec{d}$ and $\overrightarrow{br_{cm}}$, averaging over several molecules as well as time. Figure 6 contrasts G(26dFTP) and G(34dFTP), the isomers with the strongest difference in L_0 in their corresponding S-*b*-G(R_F), to show this effect. For G(26dFTP),

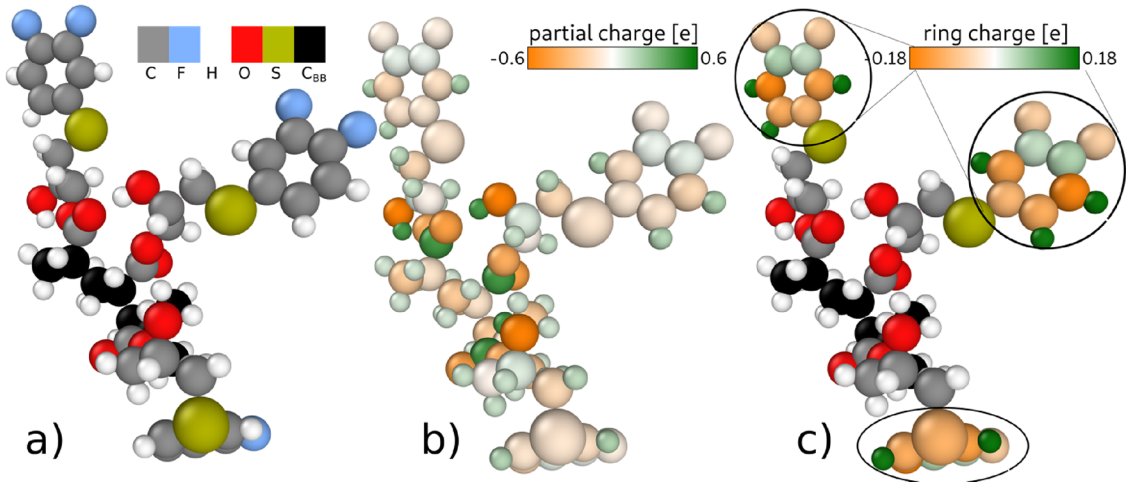

Figure 5. Schematic representation of a 3-mer of G(34dFTP) from a bulk simulation for visualization of the partial charge distribution. (a) Atom elements are indicated by their colors. C_{BB} represents the backbone carbons. (b) Colors show the partial charges on all the atoms in the 3-mer, including oxygen atoms with strong negative partial charges. (c) Colors show the partial charges of the atoms in the phenyl rings, with the partial charges of other atoms not shown.

https://doi.org/10.1021/acs.macromol.3c00630
Macromolecules 2023, 56, 4591−4601

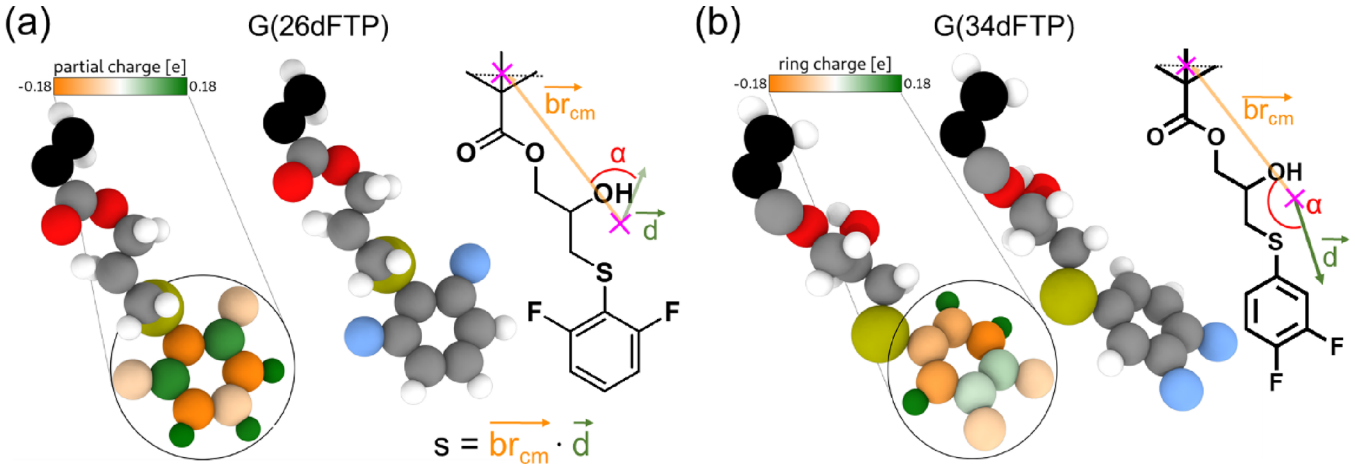

Figure 6. Schematic representation of (a) the 3-mer of G(26dFTP) and (b) 3-mer of G(34dFTP), showing the definition of the vector relations. The dipole vector $\vec{d}$ (green) is calculated from the position and partial charges of all atoms on one monomer, which is affected by the isomeric changes on the ring. The vector $\overrightarrow{br_{cm}}$ points from the center of mass of the monomer to its backbone and is defined to the side chain orientation as Galilei invariant. The inner product $s = \overrightarrow{br_{cm}} \cdot \vec{d}$ takes both the orientation and magnitude of the vectors into account.

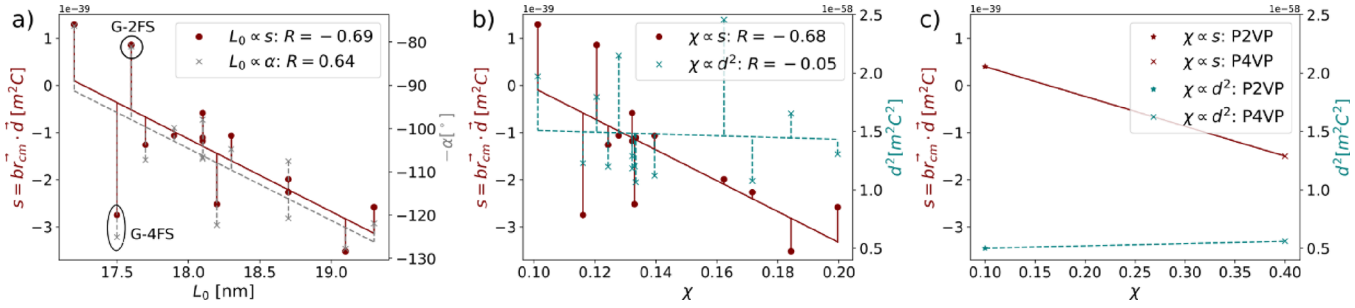

Figure 7. Visualization of the correlation between the side chain angular properties and microphase separation of S-*b*-G(R_F). The linear correlations include the best linear approximation to guide the eye as well as deviations of the data from this linear assumption. (a) Correlation between the natural lamellar period (L_0) and the inner product (s) of the dipole moment and the side chain extension, quantified with Pearson R values (left axis, maroon: $R = -0.69$) and the angle α (right axis, gray: $R = 0.64$). (b) Correlation between the estimated χ and s (left axis, maroon: $R = -0.68$). The right axis shows in teal the relation between the estimated χ and the total strength of the dipole, d^2. There is no correlation detectable ($R = -0.05$) and the linear estimation has an almost zero slope − highlighting that the total dipole strength is not indicative of microphase separation properties. (c) Same as panel (b) but with literature values of χ for S-*b*-P2VP and S-*b*-P4VP and simulated values for s and d^2.[35,36] While they have a stronger χ, the overall trend from our model system is confirmed.

the fluorine atoms are adjacent to where the sulfur atom bonds to the phenyl ring, pointing inward and shifting the dipole to the backbone, while for the G(34dFTP) isomer, the fluorine atoms are far away from the sulfur bond with the phenyl ring. This intuitive understanding is backed by our simulation results, as the average angle α between the side chain extension $\overrightarrow{br_{cm}}$ and the dipole $\vec{d}$ changes in our simulations.

Figure 7 shows the correlations between dipole orientation and microphase separation for all the fluorine-modified S-*b*-G(R_F) in this study. The correlations were quantified using Pearson R values. The p value of the reported R values are all smaller than $p < 0.015$, indicating that the reported correlations are statistically relevant. Figure 7a demonstrates the correlation between the SAXS-measured L_0 and the simulation-determined values of dipole orientation α. This analysis is independent of the estimates of χ from L_0. There is a strong correlation via a Pearson $|R| > 0.68$ but also a negative slope of the correlation making it an invertible prediction, which allows for solution of the forward and inverse problem. There are outliers from these predictions. For example, S-*b*-G(4FTP) (L_0 = 17.5 nm) has a low s value, which does not correspond with similar monofluorinated versions of S-*b*-G(FTP). Strictly speaking, there are other factors that could play a role and that are not examined here. Additionally, for this correlation, only the effect of changing the positions of the F atoms in the R_F-SH modified S-*b*-G system, where S is invariant, is considered, and it could not be determined if such a correlation holds for other second block materials. However, this correlation with the dipole-moment orientation is striking and could help engineer polymeric materials with the desired characteristic domain length scales. The inner product, s, shows a better correlation than the angle, α, which can be explained by the fact that s considers both orientation and the magnitude of dipole moment, although the latter has little correlation with χ. This analysis leads to the conclusion that the relative orientation of these vectors is more important than their magnitude. The interaction between the S side group and the G side group appears to be what drives microphase separation and leads to the difference in χ. The exact mechanism of how the orientation of side chain and dipole interact with the S block is not known. However, we can correlate the simulated relation with the experimentally measured L_0 and the derived χ, as shown in Figure 7.

https://doi.org/10.1021/acs.macromol.3c00630
Macromolecules 2023, 56, 4591−4601

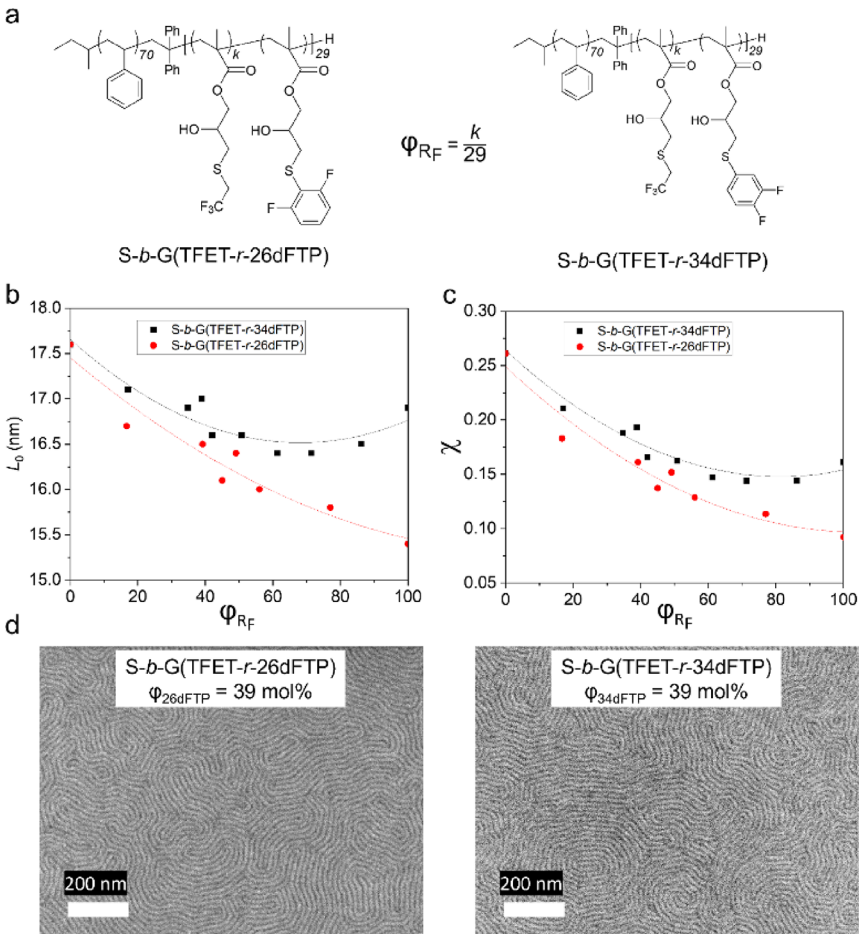

Figure 8. (a) Chemical structures of S-*b*-G(TFET-*r*-26dFTP) and S-*b*-G(TFET-*r*-34dFTP). (b) Plot of L_0 as a function of φ_{RF}. The solid lines represent the best second-order polynomial fitting. (c) Plot of χ as a function of φ_{RF}. The solid lines represent the best second-order polynomial fitting. (d) SEM images showing fingerprint features after annealing BCP thin films on a substrate functionalized with hydroxy-terminated poly(styrene-*r*-methyl methacrylate).

Figure 7b shows the correlation of s with L_0, which is measured directly, to the estimated χ value determined with eq 1. The correlation holds, which underscores that the approximations necessary to determine χ do not influence our observations. Furthermore, the χ parameter can be compared with the absolute strength of the dipole, d^2. In this case, a correlation is not found ($R = -0.05$, $p = 0.87$), which implies that the orientation of the dipole to the backbone determines the block interaction and not the absolute magnitude of the dipole.

To validate the methodology described above, analogous similar 3-mer systems of S-*b*-P2VP and S-*b*-P4VP are simulated to determine their dipole moments. S-*b*-P2VP and S-*b*-P4VP are known to exhibit significantly different microphase separation behavior while the only difference in their chemical structures is in the position of the nitrogen.[15,17,35] For S-*b*-P2VP, a squared dipole moment of $\overline{d}^2 = (5.0 \pm 1.2) \times 10^{-59}$ m^2 C^2 is obtained, which is similar to that of S-*b*-P4VP, $\overline{d}^2 = (5.6 \pm 0.9) \times 10^{-59}$ m^2 C^2. In this case, the magnitude of the dipole is not responsible for the difference in χ. Analysis of s and including the orientation of the dipole moment offers an explanation for the observed behavior. For S-*b*-P2VP, $s = (4.0 \pm 2.2) \times 10^{-40}$ m^2 C, while for S-*b*-P4VP, $s = (15 \pm 8) \times 10^{-40}$ m^2 C. These s values differ by an order of magnitude and a sign change, highlighting the contrast between the dipole properties of the molecules. Thus, the methodology presented here is sensitive to the well-known system of pyridines, and confirms the same trends observed with S-*b*-G(R_F), namely, that s and α affect χ, but the absolute strength of the dipole does not.

With this enhanced understanding of the effect of structural isomerism on χ, the potential applications of leveraging structural isomerism to alter χ and thus BCP assembly were demonstrated in the design and synthesis of two structurally isomeric BCPs with an A-*block*-(B-*random*-C) polymer architecture. For most R_F, the surface energies of the S and the G(R_F) would be sufficiently different that self-assembly with thermal annealing would not yield through-film perpendicular domains, which are desirable for template formation. Thus, an A-*block*-(B-*random*-C) architecture was used so that the two blocks of the BCP could have equal surface energies and self-assemble to form perpendicular structures, as seen before with A-*block*-(B-*random*-C) BCPs.[23,37] As shown in Figure 8*b*-Ga, S-(TFET-*r*-26dFTP) and S-*b*-G(TFET-*r*-34dFTP) were synthesized, where G-(TFET) was the B component and G(26dFTP) or G-(34dFTP) were the C component, respectively. Table S5 shows these BCPs in BigSMILES line notation.[24] A series of BCPs were synthesized with different composition ratios of the C components (φ_{26dFTP} and φ_{34dFTP}). Representative ^{1}H NMR spectra can be found in Supporting Information, Figure S15. To examine the φ needed to match the surface energies of the blocks, island-hole tests were performed by depositing the thin

https://doi.org/10.1021/acs.macromol.3c00630
Macromolecules 2023, 56, 4591−4601

film samples on a preferential substrate, cross-linked S. Detailed interpretations can be found in the literature.[23,38] At φ_{26dFTP} = 39.2 mol % and φ_{34dFTP} = 39.2 mol %, 0.5 L_0 topography features were observed, indicating both blocks wet the free surface, as shown in Supporting Information, Figure S16. This further suggests that the polymer domain-free surface interaction is not sensitive to the isomerism in our systems. It could also indicate that polymer domain-free surface interactions could still be sensitive to isomerism, but the impact is attenuated by the likely different randomness in the two polymer domains, G(TFET-*r*-26dFTP) and G(TFET-*r*-34dFTP). Nevertheless, fingerprint features were formed after annealing the BCP thin films on a substrate functionalized with hydroxy-terminated poly(styrene-*r*-methyl methacrylate), which contains 33 mol % of S.

CONCLUSIONS

A series of fluorine-substituted thiophenol isomers were used to modify a single parent block copolymer, leading to a series of SI-BCPs with identical *MW* and *Đ*, which only differed in the number and position of the F atoms. This materials platform allows for a comprehensive investigation of the sole effects of structural isomerism on the self-assembly and thermodynamics of SI-BCPs. Domain periodicity was measured with SAXS, and it revealed a significant difference across isomers, particularly for difluorine-modified SI-BCPs. The segment chain length, *a*, of the G(R_F) homopolymer is assumed to be constant and further rationalized by the measurements of R_g and R_h, which varied only by a small amount. The χ values of the SI-BCPs exhibited a larger difference, which could be attributed to the polarity or the dipole moment of the side chains modified with F atoms. Atomistic simulations were used to investigate at the molecular level the relationship between the dipole moment of the G polymer system and the effect of the position of the fluorine atoms. A distinct correlation was found between the orientation of the dipole moment and the extension of the repeat unit side chain in relation to the polymer backbone. The underlying mechanisms are beyond the scope of this manuscript. In a future study, we will expand on the insights from molecular dynamics simulations to understand the interplay between these blocks with explicitly simulated interfaces, which will provide insights into dipole alignments at interfaces as well as higher-order expansions in terms of quadrupoles that may drive further correlation terms and could be responsible for π-stacking of aromatic rings. Finally, we showed one potential patterning application of structural isomerism by designing and synthesizing two BCPs with equal surface energies. The combined experimental and simulation approach adopted here has helped develop a deeper understanding of the thermodynamics of SI-BCPs at a molecular level, which we believe will aid in the development of new materials and their applications.

METHODS AND MATERIALS

Materials. The starting materials and their sources are listed as follows: styrene (99%, Aldrich); glycidyl methacrylate (GMA, 99%, Aldrich); 1,1-diphenylethylene (DPE, 97%, Aldrich); monofluorine thiophenols: 2-fluorothiophenol (2FTP, 97%, Aldrich), 3-fluorothiophenol (3FTP, 95%, Aldrich), 4-fluorothiophenol (4FTP, 98%, Aldrich); difluorine thiophenols: 2,3-difluorothiophenol (23dFTP, 97%, Oakwood Chemical), 2,4-difluorothiophenol (24dFTP, 97%, Oakwood Chemical), 2,5-difluorothiophenol (25dFTP, 97%, Oakwood Chemical), 2,6-difluorothiophenol (26dFTP, 97%, Oakwood Chemical), 3,4-difluorothiophenol (34dFTP, 97%, TCI America), 3,5-difluorothiophenol (35dFTP, 97%, Oakwood Chemical); trifluorine thiophenols: 2,3,4-trifluorothiophenol (234tFTP, 97%, Oakwood Chemical), 2,4,6-trifluorothiophenol (246tFTP, 97%, Oakwood Chemical), 3,4,5-trifluorothiophenol (345tFTP, 97%, Oakwood Chemical); tetrafluorine thiophenol: 2,3,5,6-tetrafluorothiophenol (2356tFTP, 97%, Oakwood Chemical); pentafluorine thiophenols: 2,3,4,5,6-pentafluorothiophenol (23456pFTP, 97%, Oakwood Chemical); 2,2,2-trifluoroethanethiol (TFET, 95%, Aldrich, volatile and with very unpleasant smell); lithium hydroxide (LiOH, 98.0%, Aldrich); and tetrahydrofuran (THF, 99.9%, Fisher Chemical). A LiOH aqueous solution was freshly made before each thiol-epoxy reaction at a concentration of ~20 mg/mL in deionized water. Monomers and chemicals for anionic polymerization were thoroughly purified before use. All other chemicals were used as received.

Characterization. The number averaged molecular weight (M_n) and dispersity (*Đ*) were measured on a Shimadzu gel permeation chromatography (GPC) system equipped with a Wyatt DAWN HELEOS II multi-angle light scattering detector, a Wyatt ViscoStar III differential viscometer, a Wyatt Optilab T-rEX differential refractive index detector, and a Shimadzu SPD-M_{30}A photodiode array detector (200−800 nm). The GPC pump was a Shimadzu HPLC LC20-AD. THF with 250 ppm of BHT was used as the eluent solvent and the columns sets were 2 Agilent PLgel 5 μm MIXED-D + guard.

^{1}H NMR spectra were recorded on a Bruker AVANCE II+ 500 at room temperature. The samples were dissolved in deuterated chloroform ($CDCl_3$). ^{1}H NMR integrals were used to calculate the molar fraction of thiol addition, φ.

The values of d*n*/d*c* of the fluorinated thiophenol isomer-modified G homopolymers (G(R_F)) were measured on a Wyatt Optilab T-rEX differential refractive index detector using a laser with λ = 658.0 nm. The same solvent and temperature were used for the d*n*/d*c* and R_h measurements. The concentrations of solutions were calculated using the mass of solute and solution assuming the density of the solution is the same as that of the solvent, THF (0.889 g mL^{-1}). The measured d*n*/d*c* values are summarized in the Supporting Information, Table S2. The temperature was kept at 27 °C. Four different concentrations of polymer solutions in THF ranging from 0.3 to 4 mg mL^{-1} were used. The solvent used was identical to the eluent solvent used for the GPC measurement.

DSC was performed on a TA Discovery DSC 2500. The samples were equilibrated at 150 °C for 5 min to eliminate thermal history and then cooled to −80 °C at a rate of 10 °C min^{-1} and equilibrated for another 5 min followed by a heating ramp at a rate of 10 °C min^{-1} (Figure S14). The glass transition temperatures (T_gs) were analyzed on the second heating cycle. Thermal gravimetric analysis (TGA) was recorded on a TA Discovery TGA. The samples were equilibrated at 105 °C for 5 min to remove any moisture or possible solvent molecules trapped inside followed by a heating ramp to 600 °C at a rate of 10 °C min^{-1} under a N_2 atmosphere.

Bulk transmission small-angle X-ray scattering (SAXS) patterns were collected on a Xenocs Ganesha system with a rotating anode (Cu Kα) providing a focused X-ray beam with λ = 0.154 nm. The detector used was a hybrid pixel Dectris Pilatus 300 K 2D CMOS photon-counting detector. The samples were annealed at 150 °C for 20 h under vacuum before measurement. The exposure time was 20 min for each measurement to have a good signal-to-noise ratio.

Synthetic Procedures. Poly(glycidyl methacrylate) (G) and polystyrene-*block*-poly(glycidyl methacrylate) (S-*b*-G) were synthesized via living anionic polymerization. The synthetic procedure can be found in the literature.[23] An aliquot of S block was taken to characterize the M_n and *Đ* of S. The S-*b*-G was purified by repeated precipitation in hexanes and dried under vacuum. The purified G and S-*b*-G were characterized using ^{1}H NMR and GPC.

A typical thiol-epoxy "click" reaction proceeded as follows: To a one-neck round-bottom flask, G (200 mg, 1.41 mmol of epoxy units), 2FTP (270.5 mg, 2.11 mmol (1.5 equiv of epoxy unit)), and THF (3 g) were added. This reaction solution was then placed in an ice water bath for 5 min before adding freshly made LiOH aqueous solution

https://doi.org/10.1021/acs.macromol.3c00630
Macromolecules 2023, 56, 4591−4601

(50 μL, 0.07 equiv of epoxy unit). The mixture was then allowed to warm to room temperature and stirred for 20 h. The desired product was obtained as a white powder by precipitating the mixture in hexanes three times followed by vacuum drying. ^{1}H NMR and SEC profiles of S-*b*-G and S-*b*-G(R_F) are shown in the Supporting Information, Figures S1 and S5, respectively.

A representative thiol-epoxy "click" reaction of S-*b*-G for potential patterning applications proceeded as follows: Approximately 100 mg of the S-*b*-G parent polymer (35.3 wt % GMA units, 0.252 mmol epoxy groups) was weighed into a 20 mL glass vial, and THF (~3 mL) was added. To this, a stoichiometric amount of the difluorothiophenol toward a targeted value of φ (e.g., 13.8 mg of 34dFTP for φ = 0.38) was added to the vial. A magnetic stir bar was added, and the vial was placed in an ice bath to cool to 0 °C. A cooled aqueous solution of LiOH (~30 mg of a 20 mg mL^{-1} solution, 0.1 equiv LiOH per epoxy group) was added to the cooled reaction mixture. The solution was allowed to warm to room temperature and then stirred for 24 h. Then, the solution was again cooled on ice. The same amount of the LiOH solution was added to the vial followed by a sufficient amount of TFET to saturate the remaining epoxy functional groups (87.7 mg, 3 equiv per GMA unit), and the solution was again allowed to warm to room temperature and stirred overnight. The polymer was isolated by three precipitation cycles into hexanes from THF and dried in a vacuum oven overnight.

Molecular Dynamics Simulations. We used molecular dynamics simulations to understand the molecular conformations of the monomers on an atomistic length scale[39] and specifically to gain insights into the orientation and strength of the dipole moments of monomers in three dimensions in realistic scenarios. For the simulations, we used bulk systems of 3-mers to represent the polymer melt as a trade-off between computational effort and accuracy. We used all-atoms simulations with optimized potentials for liquid simulations (OPLS).[40] We used the BOSS tool in combination with LigParGen to generate the forcefield parameters and partial charges.[41,42] We generated the starting conditions for the system containing about 20,000 atoms − depending on the exact RF molecule − via RDkit[43] and the packmol[44] configuration that can be used for measurements. First, we simulated with a timestep of Δt = 0.002 ps in the NPT ensemble, with a constant particle number N, constant temperature T = 250 K, and a constant pressure of p = 1 bar with the OpenMM simulation tool, version 7.5.[45−47] Temperature was controlled with a Langevin thermostat with friction of $\gamma = \frac{1}{\text{ps}}$ and a Monte Carlo barostat.

After this initial step, we heated the system to 500 K at a rate of $0.01\frac{\text{K}}{\text{ps}}$ to equilibrate the molecular conformations. At this elevated temperature, we simulated in the canonical ensemble until the average center of mass diffusion of the oligomers exceeded six times the average radius of gyration to ensure relaxed conformations. From the elevated temperature, we cooled the system again at $0.01\frac{\text{K}}{\text{ps}}$ to the desired temperature of 150 °C to be comparable to experimental measurements. At this temperature, we equilibrated the system again for 1 ns before we record the trajectory of 1 ns for analysis.

The final production data was used to determine the dipole moment of each monomer $\vec{d} = \sum_{i=1}^{n} \vec{p}_i q_i$ given the positions of all atoms of the monomer and their product with partial charges. The OPLS forcefield does not support polarizability and hence this dipole moment was noninduced.

AUTHOR INFORMATION

The manuscript was written through contributions of all authors. All authors have approved the final version of the manuscript.

ASSOCIATED CONTENT

Supporting Information

The Supporting Information is available free of charge at https://pubs.acs.org/doi/10.1021/acs.macromol.3c00630.

^{1}H NMR spectrum and GPC profiles of S-*b*-G and S-*b*-G(R_F); calculation of N; summary of M_n, $Đ$, dn/dc, densities, T_gs, R_h, R_g, and DSC profiles of G and G(R_F) homopolymers; description of solution SAXS measurements and associated scans for the determination of R_g; correlation plot between experimental results including L_0, R_h, R_g, and χ and simulation results including α and s; ^{1}H NMR spectra and "island-hole" tests of S-*b*-G(TFET-*r*-34dFTP) and S-*b*-G(TFET-*r*-26dFTP); BigSMILES line notation for all final BCP variations; graph of squared internal distance $R(n)^2$ as a function of backbone carbon atoms along the chain contour n; correlation of the strong segregation theory estimation of χ with the molecular dynamics (MD)-informed estimation of χN of asymmetrically stiff blocks (PDF)

AUTHOR INFORMATION

Corresponding Authors

Juan J. de Pablo − *Pritzker School of Molecular Engineering, University of Chicago, Chicago, Illinois 60637, United States;* orcid.org/0000-0002-3526-516X; Email: depablo@uchicago.edu

Stuart J. Rowan − *Pritzker School of Molecular Engineering, University of Chicago, Chicago, Illinois 60637, United States; Department of Chemistry, University of Chicago, Chicago, Illinois 60637, United States*; Email: stuartrowan@uchicago.edu

Paul F. Nealey − *Pritzker School of Molecular Engineering, University of Chicago, Chicago, Illinois 60637, United States;* orcid.org/0000-0003-3889-142X; Email: Nealey@uchicago.edu

Authors

Hongbo Feng − *Pritzker School of Molecular Engineering, University of Chicago, Chicago, Illinois 60637, United States;* orcid.org/0000-0002-8806-6041

Ludwig Schneider − *Pritzker School of Molecular Engineering, University of Chicago, Chicago, Illinois 60637, United States;* orcid.org/0000-0002-3910-8217

Whitney Loo − *Department of Chemical and Biological Engineering, University of Wisconsin Madison, Madison, Wisconsin 53706, United States;* orcid.org/0000-0002-9773-3571

Gordon S. W. Craig − *Pritzker School of Molecular Engineering, University of Chicago, Chicago, Illinois 60637, United States;* orcid.org/0000-0002-0224-3511

Christopher Eom − *Pritzker School of Molecular Engineering, University of Chicago, Chicago, Illinois 60637, United States*

Zhongyang Wang − *Pritzker School of Molecular Engineering, University of Chicago, Chicago, Illinois 60637, United States;* orcid.org/0000-0002-3917-5268

Ricardo Ruiz − *The Molecular Foundry, Lawrence Berkeley National Lab, Berkeley, California 94720, United States*

Complete contact information is available at: https://pubs.acs.org/10.1021/acs.macromol.3c00630

Notes

The authors declare no competing financial interest.

https://doi.org/10.1021/acs.macromol.3c00630
Macromolecules 2023, 56, 4591−4601

■ ACKNOWLEDGMENTS

This research was supported by the U.S. Department of Commerce, National Institute of Standards and Technology, as part of the Center for Hierarchical Materials Design (CHiMaD). This work made use of the shared facilities at the University of Chicago Materials Research Science and Engineering Center, supported by National Science Foundation under award number DMR-2011854. H.F. acknowledges the X-ray research facilities at the University of Chicago for providing access to the state-of-the-art X-ray scattering techniques. Part of this work was carried out at the Soft Matter Characterization Facility of the University of Chicago. Work at the Advanced Light Source and the Molecular Foundry, which are DOE Office of Science User Facilities, was supported by contract DE-AC02-05CH11231. We thank Dr. Joshua Mysona for critically reading the manuscript.

■ REFERENCES

(1) Esteban, S. Liebig−Wöhler Controversy and the Concept of Isomerism. *J. Chem. Educ.* **2008**, *85*, 1201−1203.
(2) Worsfold, D. J.; Bywater, S. Anionic Polymerization of Isoprene. *Can. J. Chem.* **1964**, *42*, 2884−2892.
(3) Habibu, S.; Sarih, N. M.; Mainal, A. Synthesis and Characterisation of Highly Branched Polyisoprene: Exploiting the "Strathclyde Route" in Anionic Polymerisation. *RSC Adv.* **2018**, *8*, 11684−11692.
(4) Widmaier, J. M.; Meyer, G. C. Glass Transition Temperature of Anionic Polyisoprene. *Macromolecules* **1981**, *14*, 450−452.
(5) Jia, X.; Zhang, X.; Gong, D. 1, 2 Enriched Polymerization of Isoprene by Cobalt Complex Carrying Aminophosphory Fused (Pn3) Ligand. *J. Polym. Sci., Part A: Polym. Chem.* **2018**, *56*, 2286−2293.
(6) Bates, F. S.; Fredrickson, G. H. Block Copolymers - Designer Soft Materials. *Phys. Today* **1999**, *52*, 32−38.
(7) Drolet, F.; Fredrickson, G. H. Combinatorial Screening of Complex Block Copolymer Assembly with Self-Consistent Field Theory. *Phys. Rev. Lett.* **1999**, *83*, 4317.
(8) Suh, H. S.; Moni, P.; Xiong, S.; Ocola, L. E.; Zaluzec, N. J.; Gleason, K. K.; Nealey, P. F. Sub-10-Nm Patterning Via Directed Self-Assembly of Block Copolymer Films with a Vapour-Phase Deposited Topcoat. *Nat. Nanotechnol.* **2017**, *12*, 575−581.
(9) Kim, S. O.; Solak, H. H.; Stoykovich, M. P.; Ferrier, N. J.; De Pablo, J. J.; Nealey, P. F. Epitaxial Self-Assembly of Block Copolymers on Lithographically Defined Nanopatterned Substrates. *Nature* **2003**, *424*, 411−414.
(10) Ruiz, R.; Kang, H.; Detcheverry, F. A.; Dobisz, E.; Kercher, D. S.; Albrecht, T. R.; de Pablo, J. J.; Nealey, P. F. Density Multiplication and Improved Lithography by Directed Block Copolymer Assembly. *Science* **2008**, *321*, 936−939.
(11) Stoykovich, M. P.; Müller, M.; Kim, S. O.; Solak, H. H.; Edwards, E. W.; De Pablo, J. J.; Nealey, P. F. Directed Assembly of Block Copolymer Blends into Nonregular Device-Oriented Structures. *Science* **2005**, *308*, 1442−1446.
(12) Gaucher, G.; Dufresne, M.-H.; Sant, V. P.; Kang, N.; Maysinger, D.; Leroux, J.-C. Block Copolymer Micelles: Preparation, Characterization and Application in Drug Delivery. *J. Controlled Release* **2005**, *109*, 169−188.
(13) Zhou, C.; Segal-Peretz, T.; Oruc, M. E.; Suh, H. S.; Wu, G.; Nealey, P. F. Fabrication of Nanoporous Alumina Ultrafiltration Membrane with Tunable Pore Size Using Block Copolymer Templates. *Adv. Funct. Mater.* **2017**, *27*, 1701756.
(14) Park, C.; Yoon, J.; Thomas, E. L. Enabling Nanotechnology with Self Assembled Block Copolymer Patterns. *Polymer* **2003**, *44*, 6725−6760.
(15) Schulz, M. F.; Khandpur, A. K.; Bates, F. S.; Almdal, K.; Mortensen, K.; Hajduk, D. A.; Gruner, S. M. Phase Behavior of Polystyrene− Poly (2-Vinylpyridine) Diblock Copolymers. *Macromolecules* **1996**, *29*, 2857−2867.
(16) Zha, W.; Han, C. D.; Lee, D. H.; Han, S. H.; Kim, J. K.; Kang, J. H.; Park, C. Origin of the Difference in Order− Disorder Transition Temperature between Polystyrene-Block-Poly (2-Vinylpyridine) and Polystyrene-Block-Poly (4-Vinylpyridine) Copolymers. *Macromolecules* **2007**, *40*, 2109−2119.
(17) Han, S. H.; Lee, D. H.; Kim, J. K. Phase Behavior of Poly (2-Vinylpyridine)-Block-Poly (4-Vinylpyridine) Copolymers. *Macromolecules* **2007**, *40*, 7416−7419.
(18) Brandrup, J.; Immergut, E. H.; Grulke, E. A.; Abe, A.; Bloch, D. R., *Polymer Handbook*; Wiley New York: 1999; Vol. *89*.
(19) Hoyle, C. E.; Lowe, A. B.; Bowman, C. N. Thiol-Click Chemistry: A Multifaceted Toolbox for Small Molecule and Polymer Synthesis. *Chem. Soc. Rev.* **2010**, *39*, 1355−1387.
(20) Feng, H.; Lu, X.; Wang, W.; Kang, N.-G.; Mays, J. Block Copolymers: Synthesis, Self-Assembly, and Applications. *Polymer* **2017**, *9*, 494.
(21) Brändle, A.; Khan, A. Thiol−Epoxy 'Click' Polymerization: Efficient Construction of Reactive and Functional Polymers. *Polym. Chem.* **2012**, *3*, 3224−3227.
(22) Konuray, A. O.; Fernández-Francos, X.; Ramis, X. Analysis of the Reaction Mechanism of the Thiol−Epoxy Addition Initiated by Nucleophilic Tertiary Amines. *Polym. Chem.* **2017**, *8*, 5934−5947.
(23) Feng, H.; Dolejsi, M.; Zhu, N.; Yim, S.; Loo, W.; Ma, P.; Zhou, C.; Craig, G. S. W.; Chen, W.; Wan, L.; Ruiz, R.; de Pablo, J. J.; Rowan, S. J.; Nealey, P. F. Optimized Design of Block Copolymers with Covarying Properties for Nanolithograpy. *Nat. Mater.* **2022**, *21*, 1426−1433.
(24) Lin, T.-S.; Coley, C. W.; Mochigase, H.; Beech, H. K.; Wang, W.; Wang, Z.; Woods, E.; Craig, S. L.; Johnson, J. A.; Kalow, J. A.; Jensen, K. F.; Olsen, B. D. Bigsmiles: A Structurally-Based Line Notation for Describing Macromolecules. *ACS Cent. Sci.* **2019**, *5*, 1523−1531.
(25) Semenov, A. N. Theory of Block Copolymer Interfaces in the Strong Segregation Limit. *Macromolecules* **1993**, *26*, 6617−6621.
(26) Matsen, M. W.; Bates, F. S. Unifying Weak- and Strong-Segregation Block Copolymer Theories. *Macromolecules* **1996**, *29*, 1091−1098.
(27) Almdal, K.; Rosedale, J. H.; Bates, F. S.; Wignall, G. D.; Fredrickson, G. H. Gaussian-Coil to Stretched-Coil Transition in Block Copolymer Melts. *Phys. Rev. Lett.* **1990**, *65*, 1112−1115.
(28) Jo, S.; Jeon, S.; Jun, T.; Park, C.; Ryu, D. Y. Fluorine-Containing Styrenic Block Copolymers toward High X and Perpendicular Lamellae in Thin Films. *Macromolecules* **2018**, *51*, 7152−7159.
(29) Leibler, L. Theory of Microphase Separation in Block Co-Polymers. *Macromolecules* **1980**, *13*, 1602−1617.
(30) Sewell, J. H. A method of calculating densities of polymers. *J. Appl. Polym. Sci.* **1973**, *17*, 1741−1747.
(31) Khasat, N.; Pennisi, R. W.; Hadjichristidis, N.; Fetters, L. J. Dilute Solution Behavior of 3-Arm Asymmetric and Regular 3-and 12-Arm Polystyrene Stars. *Macromolecules* **1988**, *21*, 1100−1106.
(32) Fetters, L. J.; Lohse, D. J.; Richter, D.; Witten, T. A.; Zirkel, A. Connection between Polymer Molecular Weight, Density, Chain Dimensions, and Melt Viscoelastic Properties. *Macromolecules* **1994**, *27*, 4639−4647.
(33) Fetters, L. J.; Hadjichristidis, N.; Lindner, J. S.; Mays, J. W. Molecular-Weight Dependence of Hydrodynamic and Thermodynamic Properties for Well-Defined Linear-Polymers in Solution. *J. Phys. Chem. Ref. Data* **1994**, *23*, 619−640.
(34) Zdyrko, B.; Klep, V.; Luzinov, I. Synthesis and Surface Morphology of High-Density Poly (Ethylene Glycol) Grafted Layers. *Langmuir* **2003**, *19*, 10179−10187.
(35) Kennemur, J. G. Poly (Vinylpyridine) Segments in Block Copolymers: Synthesis, Self-Assembly, and Versatility. *Macromolecules* **2019**, *52*, 1354−1370.
(36) Sinturel, C.; Bates, F. S.; Hillmyer, M. A. High χ−LowNBlock Polymers: How Far Can We Go? *ACS Macro Lett.* **2015**, *4*, 1044−1050.

https://doi.org/10.1021/acs.macromol.3c00630
Macromolecules 2023, 56, 4591−4601

(37) Kim, S.; Nealey, P. F.; Bates, F. S. Decoupling Bulk Thermodynamics and Wetting Characteristics of Block Copolymer Thin Films. *ACS Macro Lett.* **2012**, *1*, 11−14.
(38) Peters, R. D.; Yang, X. M.; Kim, T. K.; Sohn, B. H.; Nealey, P. F. Using Self-Assembled Monolayers Exposed to X-Rays to Control the Wetting Behavior of Thin Films of Diblock Copolymers. *Langmuir* **2000**, *16*, 4625−4631.
(39) Schneider, L.; Schwarting, M.; Mysona, J.; Liang, H.; Han, M.; Rauscher, P. M.; Ting, J. M.; Venkatram, S.; Ross, R. B.; Schmidt, K. J.; Blaiszik, B.; Foster, I.; de Pablo, J. J. In Silico Active Learning for Small Molecule Properties. *Mol. Syst. Des. Eng* **2022**, 1611.
(40) Jorgensen, W. L.; Maxwell, D. S.; Tirado-Rives, J. Development and Testing of the Opls All-Atom Force Field on Conformational Energetics and Properties of Organic Liquids. *J. Am. Chem. Soc.* **1996**, *118*, 11225−11236.
(41) Dodda, L. S.; Cabeza de Vaca, I.; Tirado-Rives, J.; Jorgensen, W. L. Ligpargen Web Server: An Automatic Opls-Aa Parameter Generator for Organic Ligands. *Nucleic Acids Res.* **2017**, *45*, W331−W336.
(42) Jorgensen, W. L.; Tirado-Rives, J. Molecular Modeling of Organic and Biomolecular Systems Using Boss and Mcpro. *J. Comput. Chem.* **2005**, *26*, 1689−1700.
(43) RDKit, C *Machine Learning Software*; RDKit 2013. In 2021.
(44) Martínez, L.; Andrade, R.; Birgin, E. G.; Martínez, J. M. Packmol: A Package for Building Initial Configurations for Molecular Dynamics Simulations. *J. Comput. Chem.* **2009**, *30*, 2157−2164.
(45) Eastman, P.; Friedrichs, M. S.; Chodera, J. D.; Radmer, R. J.; Bruns, C. M.; Ku, J. P.; Beauchamp, K. A.; Lane, T. J.; Wang, L.-P.; Shukla, D.; Tye, T.; Houston, M.; Stich, T.; Klein, C.; Shirts, M. R.; Pande, V. S. Openmm 4: A Reusable, Extensible, Hardware Independent Library for High Performance Molecular Simulation. *J. Chem. Theory Comput.* **2013**, *9*, 461−469.
(46) Eastman, P.; Pande, V. Openmm: A Hardware-Independent Framework for Molecular Simulations. *Comput. Sci. Eng.* **2010**, *12*, 34−39.
(47) Eastman, P.; Swails, J.; Chodera, J. D.; McGibbon, R. T.; Zhao, Y.; Beauchamp, K. A.; Wang, L.-P.; Simmonett, A. C.; Harrigan, M. P.; Stern, C. D.; Wiewiora, R. P.; Brooks, B. R.; Pande, V. S. Openmm 7: Rapid Development of High Performance Algorithms for Molecular Dynamics. *PLoS Comput. Biol.* **2017**, *13*, No. e1005659.

https://doi.org/10.1021/acs.macromol.3c00630
Macromolecules 2023, 56, 4591−4601